FDTD Analysis of Power Deposition Patterns of an Array of Interstitial Antennas for Use in Microwave Hyperthermia

Paul C. Cherry, *Student Member, IEEE,* and Magdy F. Iskander, *Senior Member, IEEE*

Abstract—**In earlier contributions where the Method of Moments (MOM) was used to model and calculate the electromagnetic (EM) power distribution pattern in tumors heated using interstitial antennas, some modeling difficulties were encountered. This includes inaccuracies at dielectric interfaces when pulse basis functions were used for expansion and the inability to model large tumors because of the increasingly large matrices involved. In this paper, we use the Finite-Difference Time-Domain (FDTD) method to calculate EM power deposition patterns in inhomogeneous tissue models of tumors. The radiated near-field patterns from an array of uniformly and step-insulated interstitial antennas were used as incident fields on the excitation planes to calculate the scattered fields and total SAR patterns in tumors. Comparison of FDTD data with results from the Method of Moments show that FDTD solution, in this particular application, overcomes some of the modeling difficulties encountered in the Method of Moments. Results for some specific tumor geometries are also presented to show the effectiveness of the microwave interstitial heating techniques in treating large tumors. Other advantages of the FDTD method, such as improved accuracy in modeling dielectric interfaces and the ability to model large tumors, are also illustrated.**

Introduction

MICROWAVE hyperthermia using interstitial antennas provides a viable alternative to other regional and local microwave heating techniques and in many ways provides desirable heating characteristics [1]. Interstitial antennas can be used to directly heat deep-seated tumors, while minimally heating the surrounding healthy tissue. When interstitial antennas are used in conjunction with other types of treatments, such as brachytherapy, the existing surgical tracks can be used to insert interstitial antennas into the body [2], thus minimizing the patient's discomfort. Arrays of interstitial antennas offer increased heating control as well as steering capabilities of the heating pattern.

For realistic and effective evaluation of the heating characteristics of interstitial antennas, their radiation fields must be accurately determined for both uniformly and step-insulated antennas [3]–[5]. Also, since the complex permittivity of tumors may vary by as much as 25 percent from those of normal tissue [6], [7], an accurate three-dimensional (3D) model must be utilized to determine the power deposition, or SAR, pattern in tissue regions that include tumors. The results from these modeling efforts help in designing more efficient antennas and in recognizing the optimal arrangement of the antenna array elements so as to increase the therapeutic value of microwave hyperthermia treatments in a given clinical situation.

Analytical and approximate closed-form solutions of the current distribution along and the near fields radiated from uniformly and step-insulated antennas were described in earlier publications [1], [3], [8]–[10]. Excellent agreement with experimental data was also illustrated in [4]. Previous numerical modeling efforts, however, utilized the Method of Moments (MOM) [1], [3] and numerical difficulties were encountered. The Method of Moments solution, with pulse basis functions, can be accurately used to determine the power deposition in a homogeneous medium, but inaccuracies are often encountered at dielectric interfaces [11]. The degree of error depends on the difference between the complex permittivities at the interface. In order to overcome these inaccuracies, linear [12] or rooftop [13] basis functions are often needed. The use of these basis functions, however, significantly increases the size of the resulting matrices. For example, it is shown that while the linear expansion of the fields in each mathematical cell helped in improving the accuracy of the field values at boundaries and interfaces [12], it required the calculation of 12 unknowns in each mathematical cell, a matter that seriously limited the value of the method and restricted its application to electrically small objects ($ka \approx 1$) [14]. The FDTD method, on the other hand, may provide improved accuracy when modeling inhomogeneous tissue, particularly at dielectric interfaces [15], [16]. Also, because the FDTD method is an iterative procedure, it may be more suitable for dealing with large tumors.

In this paper, we examine the features of applying the FDTD to calculate SAR distribution in inhomogeneous tissue models heated using microwave interstitial antennas. Obtained results are compared with those of the Method of Moments and specific calculation examples were used to emphasize advantages of the FDTD method in this particular application.

Manuscript received September 6, 1990; revised January 14, 1992.

The authors are with the Electrical Engineering Department, University of Utah, Salt Lake City, UT 84112.

IEEE Log Number 9200857.

Method of Solution

Fig. 1 shows a typical geometry for heating a tumor with an array of interstitial antennas. The calculation of the power deposition in the tumor and the surrounding area involves basically two steps:

1. Calculation of the near-field radiation from a uniformly or step-insulated antenna. These fields are considered the incident radiation on the tumor region.
2. Calculation of the SAR pattern using an accurate 3-D model of the tumor and the surrounding tissue.

The following is a description of each of these two steps.

1. Radiation Characteristics of Interstitial Antennas

Calculation of the radiation pattern of interstitial antennas is by itself a two-step solution. The first is to determine the current and charge distributions along the antenna while the other is to calculate the radiated fields due to the current/charge distributions [1], [4], [5], [10].

Consider the uniformly and step-insulated monopole antennas shown in Fig. 2. The current distribution along these antennas can be calculated using the theory developed by R. W. P. King *et al.* [8] for insulated antennas in conductive medium. This theory utilizes an analogy with the theory of multi-section transmission lines. It simply treats sections of insulated antennas as transmission lines with complex propagation constants which accounts for the ohmic losses in the conductors as well as the radiation losses [8], [9]. Application of this procedure to multi-section interstitial antennas is described elsewhere [4], [5].

The other part of the solution involves the calculation of the radiation fields from the interstitial antennas in terms of the current and charge distributions determined as described above. A rigorous procedure is available for both uniformly insulated antennas [10] and for those of multi-section design [1].

Alternatively, an approximate model is used to find the radiated fields from the current distribution [4], [5]. This method is based on the determination of the amplitudes of a discrete set of point sources distributed along the surface of the antenna. The point sources are found based on the current distribution and are multiplied by a radiation efficiency factor. This factor is taken to represent the ability of the antenna to lose energy in the form of radiation, and is equal to α/β where the propagation constant is $k_l = \alpha + j\beta$. The radiation efficiency factor α/β is in fact proportional to the losses per wavelength [4]. This approximate procedure for calculating the radiation fields has been utilized in the present calculations.

2. FDTD 3-D Modeling of Tumors

For accurate calculation of the power deposition pattern of interstitial antennas, detailed 3-D models of tumors must be utilized. This is because, as mentioned earlier, the complex permittivity of tumors may be as much as 25 percent different from those of normal tissue [6], [7] and hence the geometry and tissue distribution of tumors must be accurately accounted for in a 3-D model. In a previous calculation [3], the Method of Moment was used for the 3-D modeling of tumors. Pulse basis functions were used to expand the fields and some difficulties were encountered. First, inaccuracies at dielectric interfaces were observed, and because of computer memory limitations, the solution was limited to small-sized tumors. To help overcome some of these difficulties, an FDTD program was written to provide 3-D models of tumors and surrounding tissue. It is hoped that the FDTD method will overcome some of the shortcomings of the Method of Moments. Following is a brief summary of the FDTD solution procedure, some of the obtained results, and an assessment of the features of the FDTD method in this particular application.

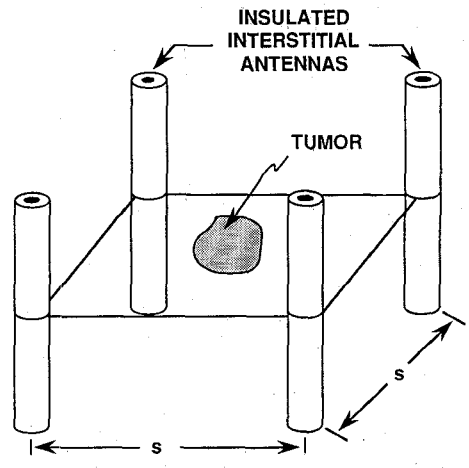

Fig. 1. Geometry of heating a tumor with a four-element array of interstitial antennas.

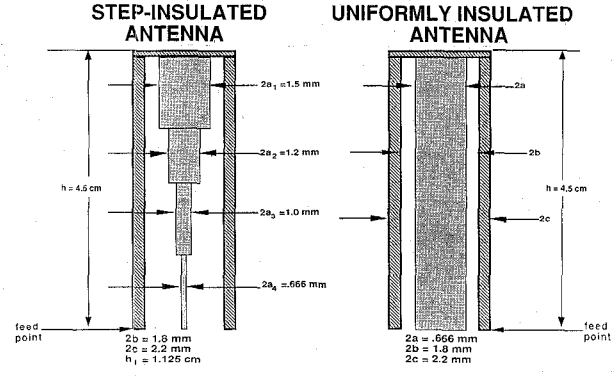

Fig. 2. Geometries of uniformly and step-insulated interstitial monopole antennas.

2.1. Yee's Algorithm

Yee [17] expressed Maxwell's curl equations in their finite-difference form. The curl equations that are used in the Yee/FDTD algorithm are

$$\nabla \times \boldsymbol{H} = \frac{\partial \boldsymbol{D}}{\partial t} + \boldsymbol{J}, \quad \nabla \times \boldsymbol{E} = -\frac{\partial \boldsymbol{B}}{\partial t} \tag{1}$$

By expressing a continuous function of space and time in its discretized form, a function at its (nth) time step can

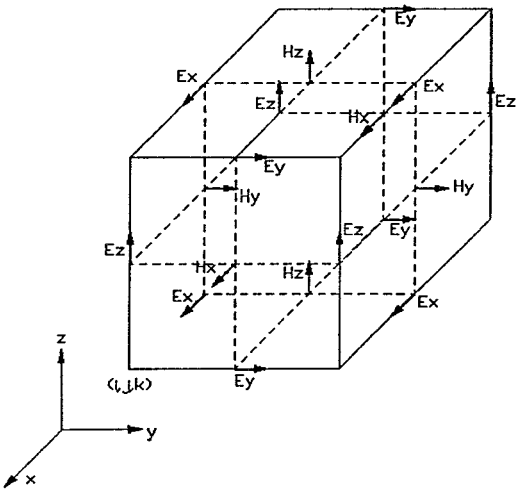

Fig. 3. Position of field components in the three-dimensional unit Yee cell. After [17].

be rewritten as

$$F^n(i, j, k) = F(i\Delta x, j\Delta y, k\Delta z, n\Delta t). \tag{2}$$

FDTD utilizes the Yee cell [17] for placement of the six electric- and magnetic-field components for computation at the nodes of the finite-difference lattice. Fig. 3 shows Yee's unit cell and the $\boldsymbol{E}$- and $\boldsymbol{H}$-field components that are positioned in the cell. The dimensions of the cell are Δx, Δy, and Δz in the x, y, and z directions, respectively. By expanding the three $\boldsymbol{E}$ and $\boldsymbol{H}$ components represented in (1) in their finite-difference approximation, using the central-difference method, for both space and time and utilizing $\Delta x = \Delta y = \Delta z = \delta$, one can obtain [17]

$$H_x^{n+(1/2)}(i, j+\tfrac{1}{2}, k+\tfrac{1}{2}) = H_x^{n-(1/2)}(i, j+\tfrac{1}{2}, k+\tfrac{1}{2}) + \frac{\Delta t}{\mu(i, j+\frac{1}{2}, k+\frac{1}{2})\,\delta}\left[\begin{array}{l} E_y^n(i, j+\frac{1}{2}, k+1) - E_y^n(i, j+\frac{1}{2}, k) \\ +E_z^n(i, j, k+\frac{1}{2}) - E_z^n(i, j+1, k+\frac{1}{2}) \end{array}\right] \tag{3a}$$

$$H_y^{n+(1/2)}(i+\tfrac{1}{2}, j, k+\tfrac{1}{2}) = H_z^{n-(1/2)}(i+\tfrac{1}{2}, j, k+\tfrac{1}{2}) + \frac{\Delta t}{\mu(i+\frac{1}{2}, j, k+\frac{1}{2})\,\delta}\left[\begin{array}{l} E_x^n(i+\frac{1}{2}, j, k) - E_x^n(i+\frac{1}{2}, j, k+1) \\ +E_z^n(i+1, j, k+\frac{1}{2}) - E_z^n(i, j, k+\frac{1}{2}) \end{array}\right] \tag{3b}$$

$$H_z^{n+(1/2)}(i+\tfrac{1}{2}, j+\tfrac{1}{2}, k) = H_z^{n-(1/2)}(i+\tfrac{1}{2}, j+\tfrac{1}{2}, k) + \frac{\Delta t}{\mu(i+\frac{1}{2}, j+\frac{1}{2}, k)\,\delta}\left[\begin{array}{l} E_x^n(i+\frac{1}{2}, j+1, k) - E_x^n(i+\frac{1}{2}, j, k) \\ +E_y^n(i, j+\frac{1}{2}, k) - E_y^n(i+1, j+\frac{1}{2}, k) \end{array}\right] \tag{3c}$$

$$E_x^{n+1}(i+\tfrac{1}{2}, j, k) = \left[\frac{1-\sigma(i+\frac{1}{2}, j, k)\,\Delta t}{\epsilon(i+\frac{1}{2}, j, k)}\right]E_x^n(i+\tfrac{1}{2}, j, k) + \frac{\Delta t}{\epsilon(i+\frac{1}{2}, j, k)\,\delta}\left[\begin{array}{l} H_z^{n+(1/2)}(i+\frac{1}{2}, j+\frac{1}{2}, k) - H_z^{n+(1/2)}(i+\frac{1}{2}, j-\frac{1}{2}, k) \\ +H_y^{n+(1/2)}(i+\frac{1}{2}, j, k-\frac{1}{2}) - H_y^{n+(1/2)}(i+\frac{1}{2}, j, k+\frac{1}{2}) \end{array}\right] \tag{4a}$$

$$E_y^{n+1}(i, j+\tfrac{1}{2}, k) = \left[\frac{1-\sigma(i, j+\frac{1}{2}, k)\,\Delta t}{\epsilon(i, j+\frac{1}{2}, k)}\right]E_y^n(i, j+\tfrac{1}{2}, k) + \frac{\Delta t}{\epsilon(i, j+\frac{1}{2}, k)\,\delta}\left[\begin{array}{l} H_x^{n+(1/2)}(i, j+\frac{1}{2}, k+\frac{1}{2}) - H_x^{n+(1/2)}(i, j+\frac{1}{2}, k-\frac{1}{2}) \\ +H_z^{n+(1/2)}(i-\frac{1}{2}, j+\frac{1}{2}, k) - H_z^{n+(1/2)}(i+\frac{1}{2}, j+\frac{1}{2}, k) \end{array}\right] \tag{4b}$$

$$E_z^{n+1}(i, j, k+\tfrac{1}{2}) = \left[\frac{1-\sigma(i, j, k+\frac{1}{2})\,\Delta t}{\epsilon(i, j, k+\frac{1}{2})}\right]E_z^n(i, j, k+\tfrac{1}{2}) + \frac{\Delta t}{\epsilon(i, j, k+\frac{1}{2})\,\delta}\left[\begin{array}{l} H_y^{n+(1/2)}(i+\frac{1}{2}, j, k+\frac{1}{2}) - H_y^{n+(1/2)}(i-\frac{1}{2}, j, k+\frac{1}{2}) \\ +H_x^{n+(1/2)}(i, j-\frac{1}{2}, k+\frac{1}{2}) - H_x^{n+(1/2)}(i, j+\frac{1}{2}, k+\frac{1}{2}) \end{array}\right] \tag{4c}$$

The 1/2's in (3) and (4) represent the field components' actual placement in the Yee cell, but the calculation is implemented on the computer as node or cell (i, j, k) in the computational lattice. From (4a)–(4c) it can be noted that each $\boldsymbol{E}$-field component for the cell (i, j, k) at the $(n + 1)$st time step depends only on the $\boldsymbol{E}$-field component's value at the previous (nth) time step and the surrounding $\boldsymbol{H}$-field components. A similar procedure is adopted for the $\boldsymbol{H}$-field components except that the magnetic field components are calculated at a 1/2-time-step difference. This provides a routine implementation of the solution procedure through Yee's cell. The values of μ, ϵ, and σ are the permeability, permittivity, and conductivity of the (i, j, k)th cell, respectively.

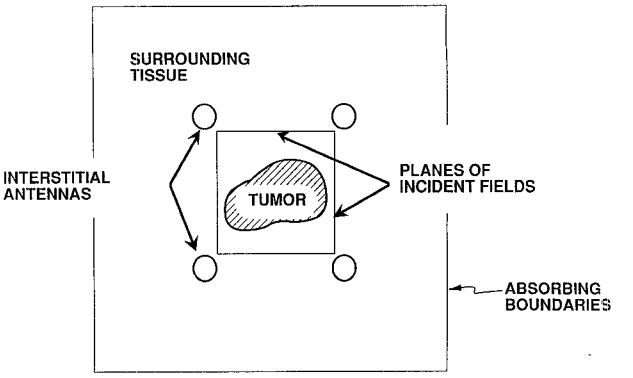

Fig. 4. Top view of the computational lattice of the FDTD techniques. The figure illustrates the location of the tumor, excitation planes, and the absorbing boundaries.

2.2. *Absorbing Boundary Conditions*

In order to model free space, boundary conditions at the computational lattice boundaries are needed. Since the computational lattice cannot be infinite for practical reasons, a finite region is used to model free space. When calculations stop at a fixed point in space, reflections occur at this computational boundary. Lattice truncation conditions at the computation boundaries which simulate those of infinite space are therefore required. These absorbing boundary conditions absorb fields that are incident on the boundaries such that reflections do not occur. Although at this time there is no perfect absorbing boundary algorithm, many approximate boundary conditions have been developed which minimize any reflections at the lattice boundaries. First- and second-order approximations have been developed for these absorbing boundary conditions, including those by Taflove and Brodwin [15], Enquist and Majda [18], and Bayliss and Turkel [19]. One of the more popular absorbing boundary conditions used and the one used for the computations in this paper is Mur's second-order boundary condition [16], [20]. It should be noted that for calculations in lossy regions, such as those presented in this paper, the absorbing boundary conditions are not as critical as for free-space scattering problems, particularly by perfectly conducting objects.

In the lossy medium case and with the appropriate selection of the size of the computational domain, the incident fields on the absorbing boundaries are expected to be significantly attenuated and hence inaccuracies associated with reflections at these boundaries are minimal. Furthermore, fields that are reflected at the absorbing boundaries attenuate as they travel back to the object, a matter that also reduces their effects.

2.3. *Computational Lattice*

Figure 4 shows the FDTD computational domain used for our modeling. The incident $\boldsymbol{E}$ field on the excitation planes was found along four planes located between the four corners of the array along the length of the antennas. The $\boldsymbol{E}$ field from all antennas in the array were summed in phasor form, using magnitude and phase, at each node in the incident plane. This phasor form of the $\boldsymbol{E}$ field was then multiplied by $e^{j\omega t}$. The real part was then taken and used as the incident field, i.e.

$$\boldsymbol{E}_{\mathrm{Inc}}(i\delta, j\delta, k\delta, n\Delta t) = \mathbf{Re}\,(\boldsymbol{E}_{\mathrm{Ant}}(i\delta, j\delta, k\delta)\, e^{j\omega n\Delta t}) \quad (5)$$

where $\boldsymbol{E}_{\mathrm{Ant}}(i\delta, j\delta, k\delta)$ is the complex phasor value of the $\boldsymbol{E}$ field at cell (i, j, k) determined from the antenna array. $n\Delta t$ is the time, ω is the radian frequency at which the calculations were made, and **Re** denotes the real part. In this paper, the Yee cell was assumed to be a cube, where $\delta x = \delta y = \delta z = \delta$. $\boldsymbol{E}_{\mathrm{Inc}}(i\delta, j\delta, k\delta, n\Delta t)$ is the value used for the incident field at the nth time step at the cell (i, j, k) in the computation lattice. δ was generally chosen to be around 2 to 5 millimeters. Δt was chosen to meet the stability criteria as set forth by Taflove [15] and is given by

$$\Delta t \leq \frac{1}{v_{\max}} \left(\frac{1}{\delta x^2} + \frac{1}{\delta y^2} + \frac{1}{\delta z^2} \right)^{-(1/2)} \quad (6)$$

using $\delta x = \delta y = \delta z = \delta$, and assuming a nonmagnetic region, (6) can be rewritten as

$$\Delta t \leq \frac{\delta \sqrt{\epsilon_{r,\min}}}{\sqrt{3}\, v_o} \quad (7)$$

where v_o is the velocity of light in air and $\epsilon_{r,\min}$ is the minimum value of ϵ_r in the computation domain. For our calculations the criteria

$$\Delta t = \frac{\delta \sqrt{\epsilon_{r,\min}}}{2 v_o} \quad (8)$$

was used. The SAR was calculated by determining the maximum $\boldsymbol{E}$ field at each node after steady state was achieved. In our calculations, steady state often occurred after 3 to 5 cycles. The SAR is defined as

$$\mathrm{SAR}\,(i\delta, j\delta, k\delta) = \frac{\sigma}{2} |\boldsymbol{E}_{\mathrm{MAX}}(i\delta, j\delta, k\delta)|^2 \quad (9)$$

where $\boldsymbol{E}_{\mathrm{MAX}}(i\delta, j\delta, k\delta)$ is the maximum steady-state electric field at cell (i, j, k) determined over a minimum of one complete cycle.

RESULTS

To check the accuracy of the FDTD calculations, SAR values for homogeneous medium were calculated and compared with those from straightforward radiation from insulated antennas. Fig. 5 shows the results for such a homogeneous medium. The computational lattice used was $40 \times 40 \times 80$ in the x, y, and z directions, respectively. The cell size used was $\delta = 2.5$ mm. The graph compares the results of the developed FDTD program with those of Trembly [10] and Tumeh [4] for an array of four uniformly insulated interstitial antennas at a frequency of 915 MHz. This figure shows good agreement, thus illustrating the accuracy of the computational procedure. Fig. 6 shows a comparison of results from the FDTD method and the Method of Moments for a cubical model of a tumor. As can be seen, the results agree quite closely with each other, thus further confirming the accuracy of the FDTD results. It should be noted that the FDTD values at nodes within and at the surface of each cubical cell shown in Fig. 6 were averaged so as to compare the FDTD results with the Method of Moments values, which are based on the pulse basis functions (average three field components in each mathematical cell).

To check the accuracy of the FDTD results at dielectric interfaces, the continuity of the tangential and normal field components at the surface interfaces between the tumor and surrounding tissue were examined. Fig. 7(a) shows the computational lattice and the three slices (A, B, and C) at which the field continuity were examined. As in many interstitial antennas, the dominant electric-field component is along the axis of the antenna (z axis in our case). Hence the field components in slice A (E_x and E_y fields) were sufficiently small to be neglected in a typical SAR calculation. Figures 7(b) and (c), therefore, show results for slices B and C only. Fig. 7(b) and (c) also give numerical values for the field components at several specific points at the dielectric interfaces. Values of the components of the electric flux density $\boldsymbol{D}$ normal to the dielectric interfaces and the tangential components of the $\boldsymbol{E}$ field are expected to be continuous. From the presented results, it may be seen that results from the FDTD solution satisfies the boundary conditions with reasonable accuracy. Larger discrepancies were observed for fields at corner cells (points R, Q, and S in Fig. 7(b) and points K, J, and L in Fig. 7(c)). An averaging process is often used to obtain an estimate of field values at dielectric corners.

With the confidence established in the capability and accuracy of the solution procedure, we proceeded to investigate the heating capabilities of an interstitial antenna array. We utilized a model of a large tumor which was computationally difficult to handle using the Method of Moments. The tumor model is shown in Fig. 8.

Fig. 9 shows the obtained SAR results for the tumor model shown in Fig. 8. The shape of the tumor was modeled after a prostrate tumor taken from a CAT scan [21]. The computational lattice used was $50 \times 50 \times 60$ cells

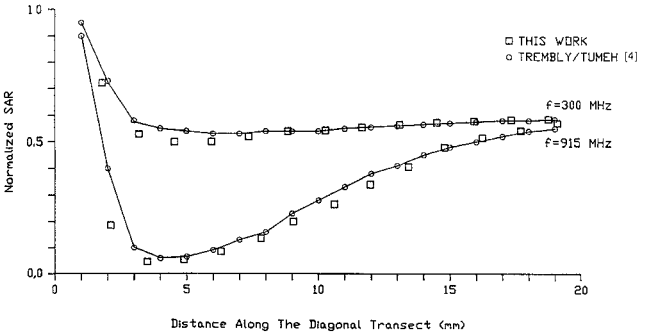

Fig. 5. Comparison of SAR results in a homogeneous tissue. Results from [4] are based on direct calculation of SAR from radiated fields from insulated antennas. Results from this work are based on using such fields on the excitation planes and the using FDTD calculations to achieve steady-state solution. The spacing between the antennas is 3 cm.

	CASE A: $\sigma_{ext} = .88$, $\sigma_{tum} = 88$, $\varepsilon_{r_{ext}} = 42\ 0$, $\varepsilon_{r_{tum}} = 42\ 0$		CASE B: $\sigma_{ext} = 88$, $\sigma_{tum} = 88$, $\varepsilon_{r_{ext}} = 42\ 0$, $\varepsilon_{r_{tum}} = 31\ 5$		CASE C: $\sigma_{ext} = 88$, $\sigma_{tum} = .66$, $\varepsilon_{r_{ext}} = 42\ 0$, $\varepsilon_{r_{tum}} = 42\ 0$	
	MOM	FD-TD	MOM	FD-TD	MOM	FD-TD
CELL 1	.92	.92	.98	.97	.95	.95
CELL 2	.83	.84	.88	.88	.86	.87
CELL 3	1.0	1.0	1.10	1.07	1.04	1.04
CELL 4	.92	.92	.98	.97	.95	.95
CELL 5	.90	.89	1.02	1.00	.94	.93
CELL 6	.81	.81	.92	.91	.85	.85
CELL 7	.98	.97	1.12	1.10	1.02	1.02
CELL 8	.90	.89	1.02	1.00	.94	.93

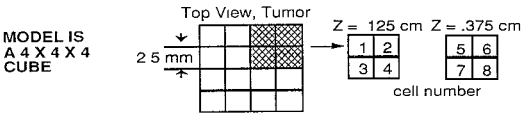

Fig. 6. Comparison between the Method of Moments and the FDTD results for a cubical model of a tumor. Results are shown for three cases concerning the dielectric constant $\epsilon_{r_{tum}}$ and conductivity σ_{tum} of the tumor, and the dielectric constant $\epsilon_{r_{ext}}$ and conductivity s_{ext} of the surrounding (external) tissue. Results are shown for one quarter of a symmetrically heated tumor model. The spacing between the antenna elements if 3 cm.

using a cubical cell with $\delta = 2.0$ mm. The tumor model contained over 10 000 cells and was assumed to have a dielectric constant of 55.0 and a conductivity of 1.45 S/m. The surrounding tissue was assumed to be muscle with a dielectric constant of 42 and a conductivity of 0.883 S/m. The antenna used for the array was a uniformly insulated antenna with a diameter of .67 mm and a length of 4.5 cm (refer to Fig. 3). The operating frequency was 915 MHz.

As indicated in earlier publications, step-insulated antennas provide several advantages over uniformly insulated ones of the same physical length [1], [4], [5]. This includes lower operating frequencies and hence improved depth of penetration and a more uniform heating pattern along the axis of the antenna. To illustrate these advantages in an inhomogeneous model of a tumor, the large tumor calculations were repeated for the case of an array of four step-insulated antennas. Figure 10 shows the obtained results at 520 MHz, which is the resonant fre-

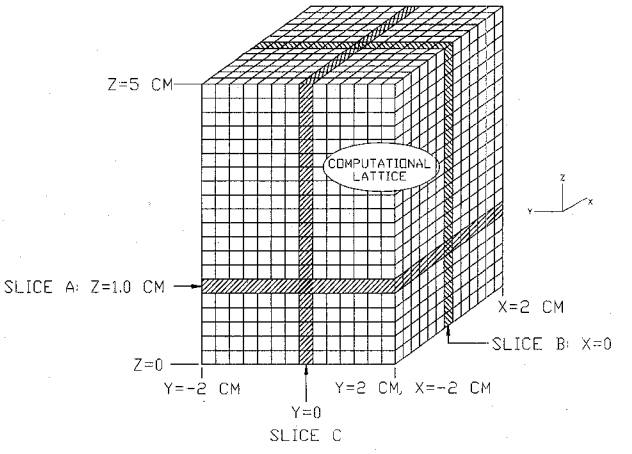

(a)

SLICE B

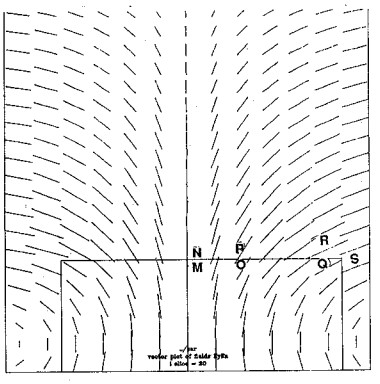

POINT	$\lvert D_z \rvert$	$\lvert D_y \rvert$	$\lvert E_z \rvert$	$\lvert E_y \rvert$
M	81.6		1.48	
N	76.0		1.81	
O	78.7		1.43	
P	73.5		1.75	
Q	52.7	11.5	.953	.210
R	48.3		1.15	
S	31.6	10.0	.752	.237

(b)

SLICE C

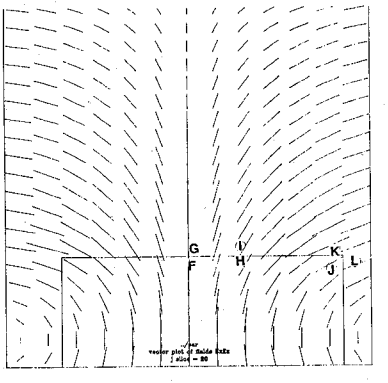

POINT	$\lvert D_z \rvert$	$\lvert D_x \rvert$	$\lvert E_z \rvert$	$\lvert E_x \rvert$
F	81.4		1.48	
G	76.0		1.81	
H	78.7		1.43	
I	73.5		1.75	
J	53.4	11.6	.971	.210
K	48.7		1.16	
L	31.4	9.8	.748	.232

(c)

Fig. 7. Electric flux density $\boldsymbol{D}$ and the electric-field intensity $\boldsymbol{E}$ components at dielectric interface between the tumor and surrounding tissues. Dielectric constant of the tumor was taken to be 55 while $\epsilon = 42$ for the surrounding tissue. The figure demonstrates the accuracy of the FDTD procedure in modeling field components at dielectric interfaces and hence in satisfying the boundary conditions. (a) Geometry of the computational lattice and slices at which specific field values were given. (b) Vector fields and tabulated values at specific points in slice b. (c) Vector fields and tabulated values at specific points in slice C.

quency of a step-insulated antenna of the same length as the uniformly insulated one, as shown in Fig. 3. Comparing Fig. 9 and Fig. 10, some of the advantages of using step-insulated antennas and operating at lower frequencies may be recognized.

At present, the FDTD program is being used to calculate EM power deposition patterns in tumor models simulating cases of clinical interest. In addition, the calculated SAR values are being utilized in a heat transfer program to calculate the temperature distribution patterns in tumors. As in earlier efforts [22], there are several parameters that critically influence the resulting temperature distribution patterns. This, for example, includes the blood-flow rate and its spatial distribution within the tumor and the thermal conductivity of the tumor and normal tissue. Therefore, results showing the utilization of the FDTD results in thermal models of the tumors will be described in a separate article to be submitted soon.

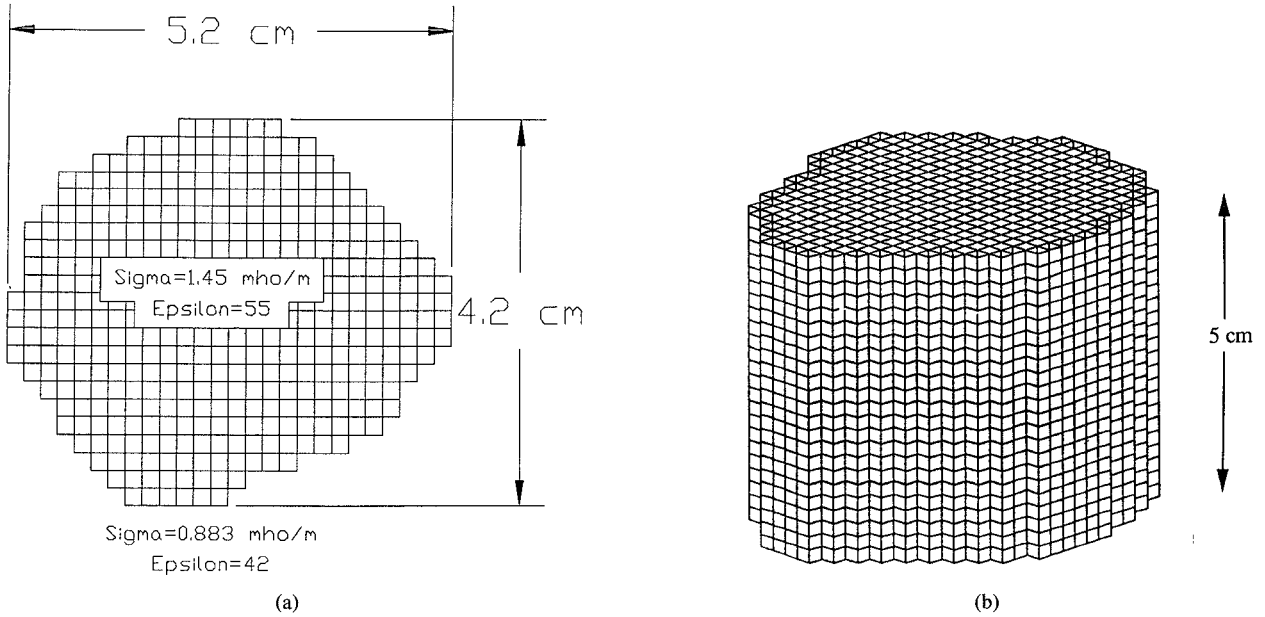

Fig. 8. Geometry and dimensions of a large tumor model used in the FDTD calculations. (a) Top view of tumor and (b) side view of the tumor geometry.

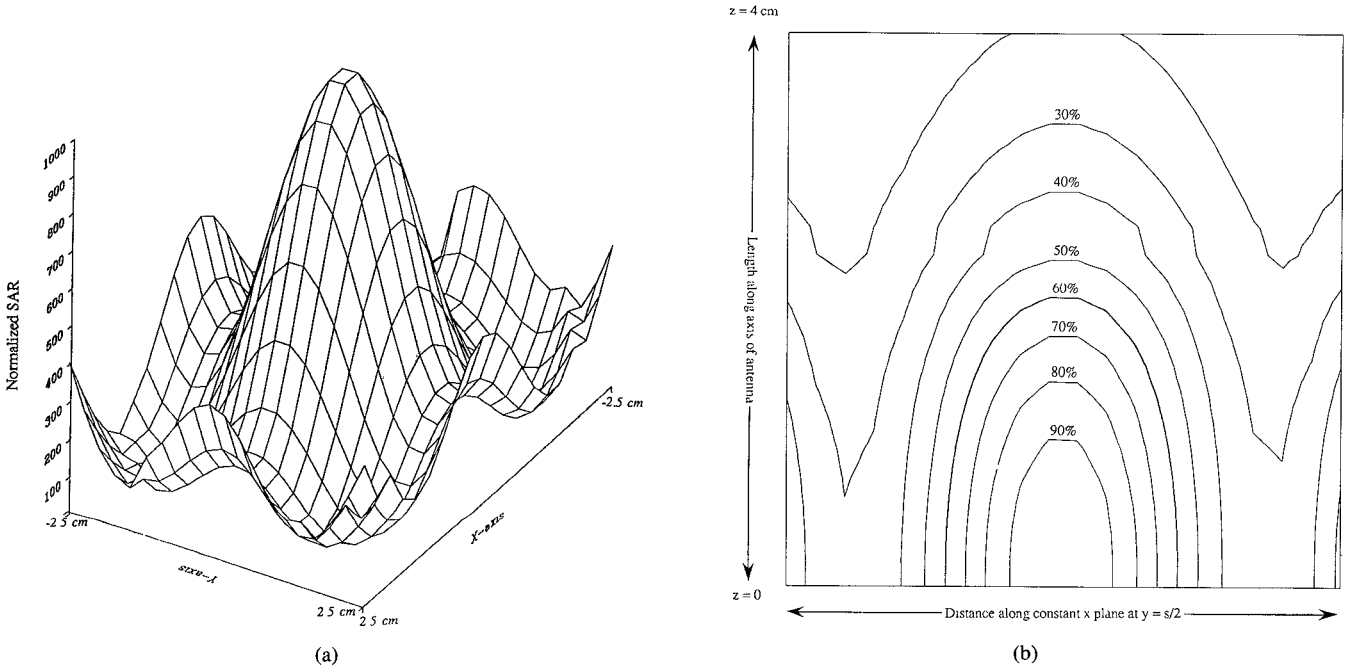

Fig. 9. (a) 3-D plot of the SAR distribution in the large tumor model shown in Fig. 8 using uniformly insulated antennas. The results show focused enhancement at the center of the tumor and relatively higher SAR values at the four corners representing the locations of the four antenna array elements. The spacing between the antenna elements is 3 cm. (b) Contour representation of the SAR distribution in a vertical plane, x = constant, placed midway between the antenna array elements, $y = s/2$.

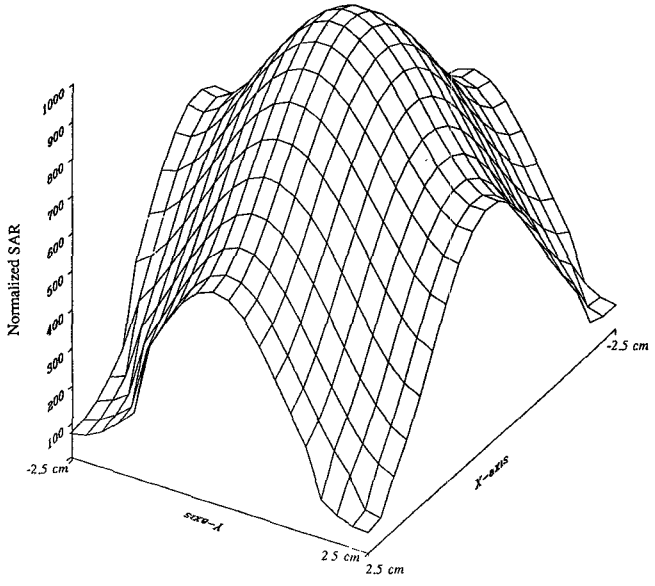

(a)

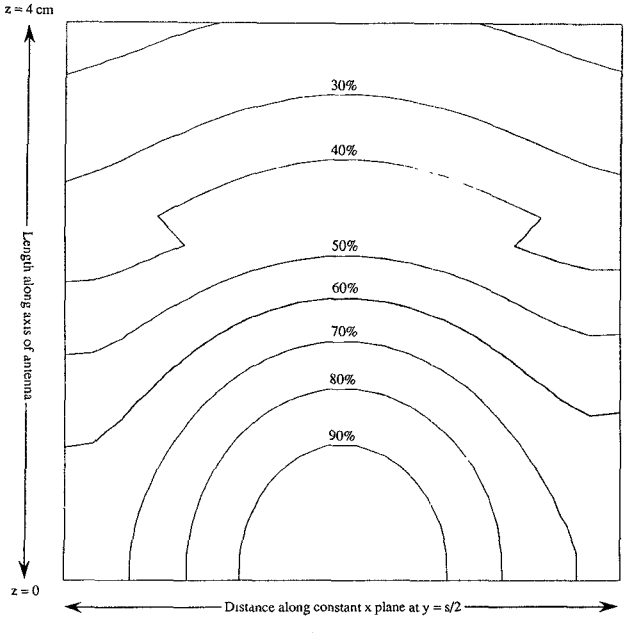

(b)

Fig. 10. (a) 3-D plot of the SAR distribution in the large tumor model using step-insulated antennas. The results were calculated at $f = 520$ MHz which is the resonant frequency of the step-insulated antenna. The results show more uniform SAR distribution as compared with those of Fig. 9. The spacing between the antenna elements if 3 cm. Results are plotted at $z = 0$. (b) Contour representation of the SAR distribution in a vertical plane, x = constant, placed midway between the antenna array elements, $y = s/2$. Calculations were made for step-insulated antennas and SAR contours are shown at $z = 0$.

Conclusion

In this paper, an FDTD program was developed to calculate the power deposition pattern of an array of interstitial antennas in an inhomogeneous tissue model. Specific calculations were made to illustrate some of the advantages of the FDTD method over other methods, such as the Method of Moments. These include improved accuracy in modeling electromagnetic fields at dielectric interfaces and the ability to handle electrically large tumors and near-field excitation by an antenna array. It is shown that while the advantage of FDTD solution in modeling large tumors was clearly demonstrated, continuity of field components at interfaces and in particular at dielectric corners are delicate quantities and should be approached with care in each problem. In the specific application of the inhomogeneous tissue model, satisfactory results were obtained at interfaces and averaging is suggested to obtain good estimates at corners.

Future use of the program includes its coupling with a companion program that uses the Finite-Difference method to calculate temperature distribution in tissue during hyperthermia treatments. The FDTD program provides the EM power deposition pattern, while the second FD program takes into account the various heat exchange mechanisms and will be used to provide temperature distributions. This will allow further design optimization of interstitial antennas, more accurate and efficient heating of tumors inside the body, and in modeling cases of specific clinical interest and presently the results in terms of the temperature distribution which is the commonly measured parameter.

References

[1] M. F. Iskander, A. M. Tumeh, and C. M. Furse, "Evaluation and optimization of the electromagnetic performance of interstitial antennas for microwave hyperthermia," *International J. of Radiation Oncology, Biology, and Physics*, vol. 18, pp. 895–902, 1990.

[2] C. T. Coughlin, E. B. Douple, J. W. Strohbehn, W. L. Eaton, B. S. Trembly, and T. Z. Wong, "Interstitial hyperthermia in combination with brachytherapy," *Radiology*, vol. 148, pp. 285–288, July 1983.

[3] C. M. Furse and M. F. Iskander, "Three dimensional electromagnetic power deposition in tumors using interstitial antennas," *IEEE Trans. Biomed. Eng.*, vol. 36, pp. 977–986, 1989.

[4] M. F. Iskander and A. M. Tumeh, "Design optimization of interstitial antennas," *IEEE Trans. Biomed. Eng.*, vol. 36, pp. 238–246, 1989.

[5] A. M. Tumeh and M. F. Iskander, "Performance comparison of available interstitial antennas for microwave hyperthermia," *IEEE Trans. Microwave Theory Tech.*, vol. 37, pp. 1126–1133, 1989.

[6] K. R. Foster and J. L. Schepps, "Dielectric properties of tumor and normal tissues at radio through microwave frequencies," *J. Microwave Power*, vol. 16, pp. 107–119, 1981.

[7] R. Peloso, D. T. Tuma, and R. K. Jain, "Dielectric properties of solid tumors during normothermia and hyperthermia," *IEEE Trans. Biomed. Eng.*, vol. BME-31, pp. 725–728, 1984.

[8] R. W. P. King, K. M. Lee, and T. F. Wu, "Theory of an insulated antenna in a dissipative medium," *Radio Science*, vol. 12, pp. 195–203, 1977.

[9] R. W. P. King and G. S. Smith, *Antenna in Matter*. Cambridge, MA: MIT Press, 1981.

[10] R. W. P. King, B. S. Trembly, and J. W. Strohbehn, "The electromagnetic field of an insulated antenna in a conduction or dielectric medium," *IEEE Trans. Microwave Theory Tech.*, vol. MTT-31, pp. 574–583, July 1983.

[11] H. Massoudi, C. H. Durney, and M. F. Iskander, "Limitations of the cubical block model of man in calculating SAR distribution," *IEEE Trans. Microwave Theory Tech.*, vol. 32, pp. 746–752, 1984.

[12] C. T. Tsai, H. Massoudi, C. H. Durney, and M. F. Iskander, "A procedure for calculating fields inside arbitrarily shaped, inhomogeneous dielectric bodies using linear basis functions with the moment method," *IEEE Trans. Microwave Theory Tech.*, vol. MTT-34, pp. 1131–1139, 1986.

[13] O. H. Schaubert, D. R. Wilton, and A. W. Glisson, "A tetrahedral

modeling method of electromagnetic scattering by arbitrarily shaped inhomogeneous bodies," *IEEE Trans. Antennas Propagat.*, vol. AP-32, pp. 75–82, 1984.

[14] M. F. Iskander, "Computational techniques in bioelectromagnetics," *Computer Physics Communications*, vol. 68, pp. 224–254, 1991.

[15] A. Taflove and M. E. Brodwin, "Numerical solutions of steady-state electromagnetic scattering problems using the time-dependent Maxwell's equations," *IEEE Trans. Microwave Theory Tech.*, vol. MTT-23, no. 8, pp. 623–629, Aug. 1975.

[16] A. Taflove and K. R. Umashankar, "Review of FDTD numerical modeling of electromagnetic wave scattering and radar cross section," *Proc. IEEE*, vol. 77, no. 5, pp. 682–698, May 1989.

[17] K. S. Yee, "Numerical solutions of initial boundary value problems involving Maxwell's equations in isotropic media," *IEEE Trans. Antennas Propagat.*, vol. AP-14, no. 3, pp. 302–307, May 1966.

[18] B. Enquist and A. Majda, "Absorbing boundary conditions for the numerical simulation of waves," *Math. Comp.*, vol. 31, pp. 629–651, July 1977.

[19] A. Bayliss and E. Turkel, "Radiation boundary conditions for wave-like equations," *Commun., Pure Appl. Math*, vol. 33, pp. 707–725, 1980.

[20] G. Mur, "Absorbing boundary conditions for the finite-difference approximation of the time-domain electromagnetic field equations," *IEEE Trans. Electromagn. Compat.*, vol. EMC-23, pp. 377–382, Nov. 1981.

[21] V. Sathiaseelan, M. F. Iskander, G. C. W. Howard, and N. M. Glechen, "Theoretically predicted effect of the phase and amplitude variations on the electromagnetics power deposition patterns for the annular-phased-array hyperthermia system," *IEEE Trans. Microwave Theory Tech.*, vol. MTT-34, pp. 514–519, 1986.

[22] M. F. Iskander and O. Khoshdel-Milani, "Numerical calculations of the temperature distribution in cross sections of the human body," *International J. of Radiation Oncology, Biology, and Physics*, vol. 10, pp. 1907–1912, 1984.

Paul C. Cherry (S'91) was born in Seattle, WA, on January 13, 1964. He received the B.S.E.E. degree from the University of Colorado in December 1986 and the M.S.E.E. degree from the University of Utah, in February 1992, where he is currently working towards the Ph.D. degree.

From 1987 until 1991, he worked for Unisys Corporation, CSD, in their Microwave and RF Design Group in Salt Lake City, Utah. His research interests include high-frequency analysis and numerical techniques in electromagnetics.

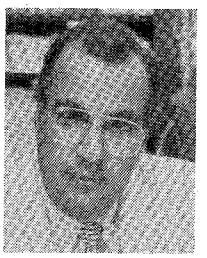

Magdy F. Iskander (S'72–M'76–SM'84) was born in Alexandria, Egypt, on August 6, 1946. He received the B.Sc. degree in Electrical Engineering from the University of Alexandria, Egypt, in 1969. He received the M.Sc. and Ph.D. degrees in 1972 and 1976, respectively, both in microwaves, from the University of Manitoba, Winnipeg, Manitoba, Canada.

In 1976, he was awarded a National Research Council of Canada Postdoctoral Fellowship at the University of Manitoba. Since 1977 he has been with the Department of Electrical Engineering at the University of Utah, Salt Lake City, Utah, where he is currently a Professor of Electrical Engineering and a Research Professor of Materials Science and Engineering. In 1981, he received the University of Utah President David P. Gardner Faculty Fellow Award and spent the academic quarter on leave as a Visiting Associate Professor at the Department of Electrical Engineering and Computer Science, Polytechnic University of New York. He spent the 1985 and 1986 summers at Chevron Oil Field Research Company, La Habra, California, as a Visiting Scientist. From September 1986 to May 1987 he spent a sabbatical leave at UCLA where he worked on the coupling characteristics of microwave integrated circuits to inhomogeneous media, and at the Harvey Mudd College where he learned about their engineering clinic program. He spent the last four months of the sabbatical leave with Ecole Superieure d'Electricite, Gif-Sur-Yvette, France, where he worked on microwave imaging. His present fields of interest include the use of numerical techniques in electromagnetics to calculate scattering by dielectric objects, antenna design for medical applications, microwave integrated circuit design, and the use of microwave methods for materials characterization and processing.

Dr. Iskander edited two special issues of the *Journal of Microwave Power*, one on "Electromagnetics and Energy Applications," March 1983, and the other on "Electromagnetic Techniques in Medical Diagnosis and Imaging," September 1983. He authored one book on *Electromagnetic Fields and Waves*, published by Prentice Hall, 1992; he edited the first CAEME software book, 1991; and coedited a third book on *Microwave Processing of Materials*, published by the Materials Research Society in 1991. The holder of seven patents, he has contributed ten chapters to seven research books, published more than 90 papers in technical journals, and made numerous presentations in technical conferences. In 1983, he received the College of Engineering Outstanding Teaching Award and the College Patent Award for creative, innovative, and practical invention. In 1984, he was selected by the Utah Section of the IEEE as the Engineer of the Year. In 1984 he received the Outstanding Paper Award from the International Microwave Power Institute, and in 1985 he received the Curtis W. McGraw ASEE National Research Award for outstanding early achievements by a university faculty member. In 1991 he received the George Westinghouse National Award for innovation in Engineering Education. In 1986 Dr. Iskander established the Engineering Clinic Program in the College of Engineering at the University of Utah. Since then the program has attracted more than 35 research projects from 16 different companies throughout the United States. He is also the director of the NSF/IEEE Center for Computer Applications in Electromagnetics Education (CAEME). He coorganized symposia on "Microwave Processing of Materials," held in conjunction with Materials Research Society meetings, spring of 1990 and 1992, in San Francisco. He also organized several workshops and special sessions in conjunction with IEEE symposia. Dr. Iskander is the editor of the *Journal on Computer Applications in Engineering Education*, published by John Wiley & Sons, Inc.